Journal of Science and Transport Technology
Journal homepage: https://jstt.vn/index.php/en

Thermally induced nonlinear instability of functionally graded plates including pores and elastic edge restraint

Hoang Van Tung[1], Vu Thanh Long[2], Duong Thi Ngoc Thu[3,*]
[1]Faculty of Civil Engineering, Hanoi Architectural University, 129 Tran Phu, Ha Dong, Hanoi, Vietnam
[2]Faculty of Civil Engineering, University of Transport Technology, 54 Trieu Khuc Street, Thanh Liet Ward, Hanoi 100000, Vietnam
[3]RIMAS Research Group (Resilience & Innovative Materials for Smart Infrastructures), University of Transport Technology, 54 Trieu Khuc Street, Thanh Liet Ward, Hanoi 100000, Vietnam

Article info
Type of article:
Original research paper

DOI:
https://doi.org/10.58845/jstt.utt.2026.en.6.2.37-55

***Corresponding author:**
Email address:
thudtn@utt.edu.vn

Received: 10/10/2025
Received in Revised Form: 04/12/2025
Accepted: 18/12/2025

Abstract: This study peruses the thermally induced nonlinear instability of rectangular plates made up functionally graded material (FGM) with porosity and elastic edge restraint. The pores are distributed in FGM via even and uneven patterns. The temperature-dependent (T-D) properties of constitutive materials are considered and effective properties of porous FGM are evaluated adopting a modification of mixture rule. Fundamental equations of nonlinear instability problem are derived employing first order shear deformation theory (FSDT) incorporating geometric imperfection and interactive pressure from two-parameter foundation. Analytical solutions of transverse displacement, stress function along with rotations are used to fulfil simply supported conditions on boundary edges and Galerkin procedure combined with an iterative process are employed to obtain critical temperatures and post-buckling paths. Parametric studies explore that porosity beneficially influences the buckling withstanding and post-buckling strength of thermally loaded FGM plates. In contrast, tangential constraints of edges have deteriorative effects on nonlinear instability of porous FGM plates undergoing thermal loadings.

Keywords: Nonlinear stability, Porosity, Thermal load, Tangential edge constraints.

1. Introduction

Owing to excellent features, functionally graded material (FGM) drew attention of many scientists in various fields. Outstanding properties of FGM result from prominent characteristics of constituent materials, such as very high stiffness along with very low thermal expansion of ceramic and ductile feature of metal. Due to these advanced properties along with good integrity, FGMs are extensively applied in structural components, especially in thermally loaded structures. Zhao et al. [1] utilized the FSDT along with kp-Ritz method to explore the buckling response of FGM plates subjected to compression and thermal loadings. Based on higher order shear deformation theory (HSDT) and adjacent equilibrium criterion, Shariat and Eslami [2] analyzed the linear instability problem of thick FGM plates loaded by uniaxial compression and high temperature. Explicit form solution for instability

problem of thick FGM plates reposing on elastic foundations under action of compressive loads was provided by Thai and Kim [3] employing the HSDT and neutral plane place. Analytical studies on the nonlinear instability of thin and shear deformable FGM rectangular plates subjected to mechanical and thermal loadings have been carried out by Tung and Duc [4, 5]. Numerical studies on the vibrational and instability behaviors of thick FGM plates were performed in works [6, 7] applying finite element method (FEM).

Since FGM structures are usually exposed to severe temperatures, thermally induced instability of FGM components are problems of essential importance. Using different plate theories and adjacent equilibrium criterion, linear stability problems of FGM plates with various thicknesses exposed to high temperatures were dealt with by Javaheri and Eslami [8, 9] and Lanhe [10]. Employing HSDT and asymptotic solutions, Shen [11] given results for post-postbuckling analysis of mid-plane symmetric FGM plates undergoing thermal loadings. An analytical study on thermoelastic instability response of FGM plates was carried out by Bodaghi and Saidi [12]. A numerical analysis on thermal instability behavior of FGM plates was performed by Tran et al. [13] utilizing isogeometric formulation. Making use of an analytical approach, Tung [14] investigated the nonlinear instability of FGM sandwich plates rested on elastic foundations under combination of compression and temperature. Using a modified FSDT and FEM, thermal instability and post-buckling problems of FGM flat and curved panels were treated by Trabelsi et al. [15, 16] and Hajlaoui et al. [17]. Do and Lee [18] employed a quasi-3D HSDT and meshless method to compute critical buckling temperatures of FGM plates loaded by thermal environments. The HSDT–based analytical solution was utilized in the work of Dong et al. [19] examining the nonlinear instability of FGM plates with oblique stiffeners and interaction with nonlinear foundation loaded by axial compression and lateral pressure. Based on some numerous plate theories and methods, the linear instability and post-buckling responses of composite plates with nanotube reinforcement undergoing elevated temperature have been analyzed in studies [20-25].

Pores can arise in the fabrication process of FGM and affect the characteristics of this composite. As a result, the impacts of pores on the static and dynamic behaviors of FG elements should be considered. The linear and nonlinear vibrational analyses of thin and shear deformable FG beam components including pore imperfection were performed in papers [26, 27]. Gupta and Talha [28] taken up a numerical approach with finite elements to analyze the impacts of geometric and pore imperfections on the linear instability of FGM plates undergoing mechanical loadings. An analytical solution and HSDT are employed in analysis of Cong et al. [29] looking at the nonlinear buckling of FGM plates with pores undergone uniaxial compressive load and thermal environment. In the study of Trinh et al. [30], a semi-analytical solution with Monte Carlo procedure was employed for stochastic instability problem of FGM plates with pores. Cuong et al. [31] made use of a isogeometric method for nonlinear instability problem of FGM microplates with pores under thermal loadings. Thermally induced nonlinear instability behavior of FGM nanobeams with porosity and imperfect geometry was examined by Salari et al. [32] taking up Timoshenko theory and Ritz solution. Dhuria et al. [33] explored the effects of pores on the static and buckling responses of FGM plates under simply supported condition on all edges utilizing Navier solution technique. Based on the FSDT and an analytical approach, the nonlinear buckling analysis of FG-GPLRC circular plates under thermal loading was executed by Phuong et al. [34]. Quan et al. [35] taken up the FSDT–based analytical solution to deal with the linear instability problem of sandwich FGM cylindrical shells with porous core under axial compression. Nonlinear buckling analyses of FGM circular cylindrical shells

with pores and tangential constraints of boundary edges under elevated temperature and thermomechanical loading were treated by Long and Tung [36, 37] utilizing a FSDT and double term solution of transverse displacement. Recently, the influences of pores on the linear and nonlinear instability problems of FGM toroidal shell segments, spherical shells, circular plates and sandwich cylindrical shells under elevated temperatures and lateral pressure have been investigated in studies [38-41]. It is evident from the literature that, there is an absence of study on instability of FGM plates including pore and elastic edge restraint subjected to thermal loads.

To fill the gap in the preceding studies, the simultaneous influences of porosity, in-plane edge constraints, geometric imperfection and foundation interaction on the nonlinear buckling and post-buckling of FGM plates exposed to uniform temperature rise are scrutinized in the present study. The effective properties of porous FGM are estimated adopting a modified version of the linear mixture rule. Mathematical derivations are implemented on the basis of FSDT incorporating geometric nonlinear terms and the interactive pressure from two-parameter foundation. The analytical solutions of deflection and stress function are used and Galerkin procedure in combination with an iteration process are employed to evaluate critical temperatures and post-buckling temperature–deflection paths. Parametric studies find that pores and flexible boundary constraints lead to beneficial and detrimental influences on the stability of thermally loaded FGM plates, respectively.

2. FGM plate model and material properties

The present work considers a rectangular plate of length, width and thickness dimensions are a, b and h, respectively, as sketched in Fig. 1. The plate is reposed on an elastic foundation and placed in a Cartesian system of coordinates which origin locates on the mid-surface at a corner and x, y, z axes are in the length, width, thickness directions, respectively.

The plate is made of porous FGM, namely, metal, ceramic and pores. The volume percentages of materials are graded continuously across the thickness direction according to a power law function as [1, 11]

$$V_m = \left(\frac{1}{2}+\frac{z}{h}\right)^N,\ V_c = 1 - V_m \tag{1}$$

where N is a non-negative value known as index of volume fraction and, herein, subscripts m and c respectively imply metal and ceramic. Because of the presence of pores, the effective properties P_{eff} of porous FGM can be calculated adopting a modification of linear mixture rule as [26]

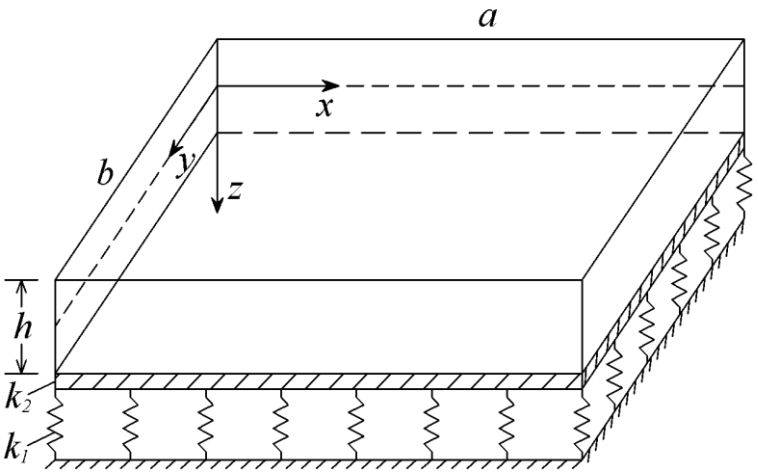

Fig. 1. Dimensions and coordinates of a plate resting on a Pasternak elastic foundation

$$P_{eff} = P_m\left(V_m - \frac{\xi}{2}\right) + P_c\left(V_c - \frac{\xi}{2}\right) \tag{2}$$

where ξ is a small value known as volume fraction of pores and P implies a particular property such

as modulus of elasticity and thermal expansion coefficient (TEC). When $\xi = 0$ FGM is free from pores and called perfect FGM. In this study, pores are distributed into the FGM according to even and uneven patterns, as sketched in Fig. 2. Combining Eqs. (1) and (2) yields the effective elastic modulus E and effective TEC α of porous FGM as [26]

Eq. (3a)

Eq. (3b)

where χ receives values 0 and 1 for even and uneven patterns of pores distribution, respectively, and effect of temperature T on material properties is incorporated. Since dependence of Poisson's ratios on temperature and position is marginal, it is assumed that Poisson ratio ν of FGM with pores is a constant.

3. Theoretical formulations

In the present work, the FSDT is applied for mathematical formulations of thermal postbuckling problem of moderately thick FGM plates incorporating the effects porosity and geometric imperfection. Within the framework of the FSDT, the strain components at a distance z from the middle plane are given as

Eq. (4)

where Eq. (5)

with u, v, w are displacement components in the x, y, z coordinates of a point on the mid-surface, respectively, and ϕ_x, ϕ_y are rotations of a normal to mid-plane about y, x exes, respectively.

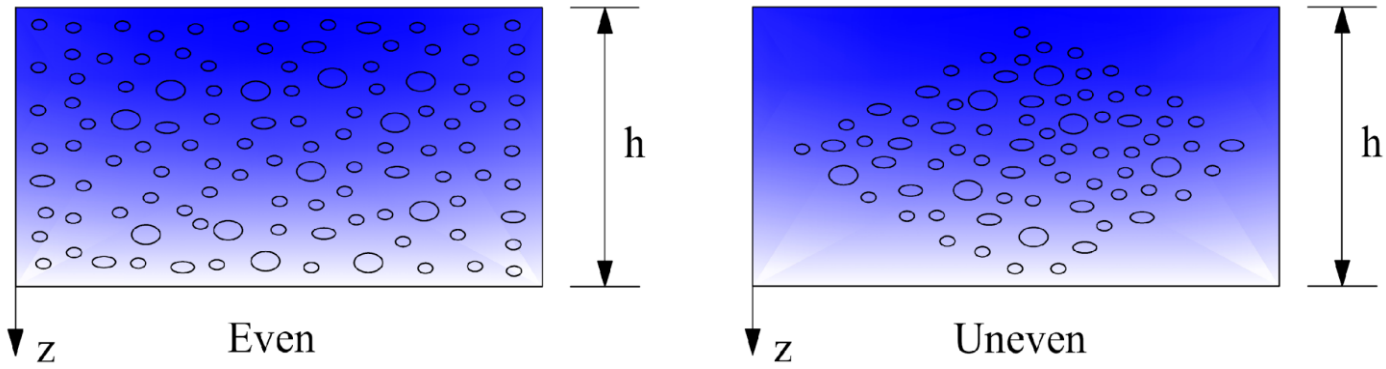

Fig. 2. Porosity distribution patterns in FGM plate

$$E(z,T) = [E_m(T) - E_c(T)]\left(\frac{1}{2} + \frac{z}{h}\right)^N + E_c - \frac{\xi}{2}[E_m(T) + E_c(T)]\left(1 - 2\chi\frac{|z|}{h}\right) \quad (3a)$$

$$\alpha(z,T) = [\alpha_m(T) - \alpha_c(T)]\left(\frac{1}{2} + \frac{z}{h}\right)^N + \alpha_c - \frac{\xi}{2}[\alpha_m(T) + \alpha_c(T)]\left(1 - 2\chi\frac{|z|}{h}\right) \quad (3b)$$

$$\begin{pmatrix}\varepsilon_x\\ \varepsilon_y\\ \gamma_{xy}\end{pmatrix} = \begin{pmatrix}\varepsilon_x^0\\ \varepsilon_y^0\\ \gamma_{xy}^0\end{pmatrix} + z\begin{pmatrix}\varepsilon_x^1\\ \varepsilon_y^1\\ \gamma_{xy}^1\end{pmatrix}, \begin{pmatrix}\gamma_{xz}\\ \gamma_{yz}\end{pmatrix} = \begin{pmatrix}\phi_x + w_{,x}\\ \phi_y + w_{,y}\end{pmatrix} \quad (4)$$

$$\begin{pmatrix}\varepsilon_x^0\\ \varepsilon_y^0\\ \gamma_{xy}^0\end{pmatrix} = \begin{pmatrix}u_{,x} + w_{,x}^2/2\\ v_{,y} + w_{,y}^2/2\\ u_{,y} + v_{,x} + w_{,x}w_{,y}\end{pmatrix}, \begin{pmatrix}\varepsilon_x^1\\ \varepsilon_y^1\\ \gamma_{xy}^1\end{pmatrix} = \begin{pmatrix}\phi_{x,x}\\ \phi_{y,y}\\ \phi_{x,y} + \phi_{y,x}\end{pmatrix} \quad (5)$$

Stress components accounting for temperature effects are defined via constitutive relations as

$$\sigma_x = \frac{E}{1-\nu^2}\left[\varepsilon_x + \nu\varepsilon_y - (1+\nu)\alpha\Delta T\right] \quad (6)$$

$$\sigma_y = \frac{E}{1-\nu^2}\left[\varepsilon_y + \nu\varepsilon_x - (1+\nu)\alpha\Delta T\right]$$

$$(\sigma_{xy}, \sigma_{xz}, \sigma_{yz}) = \frac{E}{2(1+\nu)}(\gamma_{xy}, \gamma_{xz}, \gamma_{yz})$$

in which $\Delta T = T - T_0$ is uniform temperature rise

compared to an reference temperature T_0 for which the plate is assumed to have no thermal strains. In the present analysis T_0 is chosen to be room temperature.

Membrane force intensities N_{ij}, transverse shear forces Q_x, Q_y and moment intensities M_{ij} are computed through stress components and expressed in the form

Eq. (7)

in which

Eq. (8)

and K_S symbols coefficient of shear correction which is taken to be $5/6$ in the present analysis.

By using a stress function $f(x,y)$ determined such as $N_x = f_{,yy}$, $N_y = f_{,xx}$, $N_{xy} = -f_{,xy}$ and accounting for interactive pressures from elastic foundation, equation of nonlinear equilibrium of porous FGM plates is written as the following [14]

Eq. (9)

with $\nabla^2 = \frac{\partial^2}{\partial x^2} + \frac{\partial^2}{\partial y^2}$ is Laplace operator, $D = \frac{E_1 E_3 - E_2^2}{E_1(1-\nu^2)}$, $w^*(x,y)$ is a known function characterizing initial geometric imperfection, whereas k_1 and k_2 are stiffness parameters of Winkler–Pasternak elastic foundations.

Equation of strain compatibility of a FGM plate with pores can be written in terms of the stress function and deflection as [4, 5, 14]

Eq. (10)

All boundary edges of porous FGM rectangular plate are assumed to be simply supported and constrained against tangential displacements. The corresponding mathematical expressions are taken in the form

Eq. (11a), Eq. (11b)

in which N_{x0} and N_{y0} are reactive force resultants induced at boundary edges and are related with corresponding end-shriveling components of displacements as [14, 23]

Eq. (12)

where c_1 and c_2 are respectively stiffness parameters of in-plane restraints at boundary edges $x = 0, a$ and $y = 0, b$. After solving Eqs. (5) and (7) for $\partial u / \partial x$ and $\partial v / \partial y$, Eq. (12) is rewritten in the form

Eq. (13a), Eq. (13b)

4. Solution procedure

To fulfill simply supported conditions at boundary edges, analytical solutions are chosen as the following [5, 14]

Eq. (14a), Eq. (14b), Eq. (14c)

where W and μ are amplitudes of the deflection and imperfection, respectively, $\beta_m = m\pi / a$, $\delta_n = n\pi / b$ with $m,n = 1,2,\ldots$, whereas $A_i\,(i = 1 \div 3)$ and $B_j\,(j = 1,2)$ are coefficients to be determined. By placing the Eqs. (14a) and (14b) into the Eq. (10), we obtain the coefficients A_i $(i = 1 \div 3)$ in the expression of stress function as

Eq. (15)

By setting the solutions (14b) and (14c) into the last two among five equations of equilibrium equations and executing mathematical transformations as indicated in the works [5, 24], we receive the coefficients in the rotations as

Eq. (16)

in which quantities d_{ij} $(i = 1,2\,;\, j = 1 \div 3)$ are given in Eq. (A1) in the Appendix section.

By substituting the Eqs. (14a) and (14b) into the equation of equilibrium (9) and employing Galerkin procedure to the received one, we obtain the following equation

Eq. (17)

where

Eq. (18)

and coefficients a_{k1} $(k = 1 \div 3)$ can be found in Eq. (A2) in the Appendix section.

By putting the solution expressions (14) into the Eqs. (13), the following results of reactive force

resultants are obtained

Eq. (19a), Eq. (19b)

where $G=\frac{1}{h}\int_{-h/2}^{h/2} E\alpha dz$ and coefficients s_{ij} ($i=1\div 2$, $j=1\div 3$) are given in Eq. (A4) in Appendix.

By introducing Eqs. (19) into Eq. (17), we obtain

Eq. (20)

$$\begin{aligned}
(N_x,M_x)&=\frac{1}{1-\nu^2}\left[(E_1,E_2)\left(\varepsilon_x^0+\nu\varepsilon_y^0\right)+(E_2,E_3)\left(\varepsilon_x^1+\nu\varepsilon_y^1\right)\right]-\frac{(\Phi_0,\Phi_1)}{1-\nu}\\
(N_y,M_y)&=\frac{1}{1-\nu^2}\left[(E_1,E_2)\left(\varepsilon_y^0+\nu\varepsilon_x^0\right)+(E_2,E_3)\left(\varepsilon_y^1+\nu\varepsilon_x^1\right)\right]-\frac{(\Phi_0,\Phi_1)}{1-\nu}\\
(N_{xy},M_{xy})&=\frac{1}{2(1+\nu)}\left[(E_1,E_2)\gamma_{xy}^0+(E_2,E_3)\gamma_{xy}^1\right]\\
(Q_x,Q_y)&=\frac{E_1K_S}{2(1+\nu)}\left[(\phi_x+w_{,x}),(\phi_y+w_{,y})\right]
\end{aligned} \tag{7}$$

$$(E_1,E_2,E_3)=\int_{-h/2}^{h/2}E\left(1,z,z^2\right)dz\,,\ (\Phi_0,\Phi_1)=\int_{-h/2}^{h/2}E\alpha\Delta T(1,z)\,dz \tag{8}$$

$$\begin{aligned}
&D\nabla^4 w+\frac{2(1+\nu)}{E_1K_S}D\nabla^2\left[f_{,yy}\left(w_{,xx}+w^*_{,xx}\right)-2f_{,xy}\left(w_{,xy}+w^*_{,xy}\right)+f_{,xx}\left(w_{,yy}+w^*_{,yy}\right)-k_1w+k_2\left(w_{,xx}+w_{,yy}\right)\right]\\
&\qquad-\left[f_{,yy}\left(w_{,xx}+w^*_{,xx}\right)-2f_{,xy}\left(w_{,xy}+w^*_{,xy}\right)+f_{,xx}\left(w_{,yy}+w^*_{,yy}\right)\right]+k_1w-k_2\left(w_{,xx}+w_{,yy}\right)=0
\end{aligned} \tag{9}$$

$$\nabla^4 f-E_1\left(w^2_{,xy}-w_{,xx}w_{,yy}+2w_{,xy}w^*_{,xy}-w_{,xx}w^*_{,yy}-w_{,yy}w^*_{,xx}\right)=0 \tag{10}$$

$$w=\phi_y=M_x=0\,,\ N_x=N_{x0}\ \text{at}\ x=0,\ a \tag{11a}$$

$$w=\phi_x=M_y=0\,,\ N_y=N_{y0}\ \text{at}\ y=0,\ b \tag{11b}$$

$$N_{x0}=-\frac{c_1}{ab}\int_0^a\int_0^b\frac{\partial u}{\partial x}dxdy\ ,\ N_{y0}=-\frac{c_2}{ab}\int_0^a\int_0^b\frac{\partial v}{\partial y}dxdy \tag{12}$$

$$N_{x0}=-\frac{c_1}{ab}\int_0^a\int_0^b\left[\frac{1}{E_1}\left(f_{,yy}-\nu f_{,xx}\right)-\frac{E_2}{E_1}\phi_{x,x}-\frac{1}{2}w^2_{,x}-w_{,x}w^*_{,x}+\frac{\Phi_0}{E_1}\right]dxdy \tag{13a}$$

$$N_{y0}=-\frac{c_2}{ab}\int_0^a\int_0^b\left[\frac{1}{E_1}\left(f_{,xx}-\nu f_{,yy}\right)-\frac{E_2}{E_1}\phi_{y,y}-\frac{1}{2}w^2_{,y}-w_{,y}w^*_{,y}+\frac{\Phi_0}{E_1}\right]dxdy \tag{13b}$$

$$w=W\sin\beta_m x\sin\delta_n y\,,\ w^*=\mu h\sin\beta_m x\sin\delta_n y \tag{14a}$$

$$f=A_1\cos 2\beta_m x+A_2\cos 2\delta_n y+A_3\sin\beta_m x\sin\delta_n y+\frac{1}{2}N_{x0}y^2+\frac{1}{2}N_{y0}x^2 \tag{14b}$$

$$\phi_x=B_1\cos\beta_m x\sin\delta_n y\,,\ \phi_y=B_2\sin\beta_m x\cos\delta_n y \tag{14c}$$

$$A_1=\frac{E_1\delta_n^2}{32\beta_m^2}W\left(W+2\mu h\right),\ A_2=\frac{E_1\beta_m^2}{32\delta_n^2}W\left(W+2\mu h\right),\ A_3=0 \tag{15}$$

$$B_1=\frac{d_{13}d_{22}-d_{12}d_{23}}{d_{11}d_{22}-d_{12}^2}W\,,\ B_2=\frac{d_{23}d_{11}-d_{21}d_{13}}{d_{11}d_{22}-d_{12}^2}W \tag{16}$$

$$a_{11}\overline{W}+a_{21}\left(m^2B_a^2\overline{N}_{x0}+n^2\overline{N}_{y0}\right)\left(\overline{W}+\mu\right)+a_{31}\overline{W}\left(\overline{W}+\mu\right)\left(\overline{W}+2\mu\right)=0 \tag{17}$$

$$B_a = \frac{b}{a},\ \left(\overline{W},\bar{N}_{x0},\bar{N}_{y0}\right) = \frac{1}{h}\left(W,N_{x0},N_{y0}\right) \quad (18)$$

$$\bar{N}_{x0} = s_{11}\overline{W} + s_{12}\overline{W}\left(\overline{W}+2\mu\right) - s_{13}G\Delta T \quad (19a)$$

$$\bar{N}_{y0} = s_{21}\overline{W} + s_{22}\overline{W}\left(\overline{W}+2\mu\right) - s_{23}G\Delta T \quad (19b)$$

$$\Delta T = \frac{a_{11}}{a_{21}\left(m^2B_a^2s_{13}+n^2s_{23}\right)G}\frac{\overline{W}}{\overline{W}+\mu} + \frac{m^2B_a^2s_{11}+n^2s_{21}}{\left(m^2B_a^2s_{13}+n^2s_{23}\right)G}\overline{W} + \frac{a_{21}\left(m^2B_a^2s_{12}+n^2s_{22}\right)+a_{31}}{a_{21}\left(m^2B_a^2s_{13}+n^2s_{23}\right)G}\overline{W}\left(\overline{W}+2\mu\right) \quad (20)$$

This equation describes the nonlinear relationship between thermal loading and dimensionless maximum transverse displacement of FGM plates including porosity, geometric imperfection and elastic constraints of boundary edges under uniform temperature rise. Bifurcation buckling response can take place for geometrically perfect plates ($\mu = 0$) and buckling thermal loadings are obtained as

$$\Delta T_b = \frac{a_{11}}{a_{21}\left(m^2B_a^2s_{13}+n^2s_{23}\right)G} \quad (21)$$

As indicated in previous works [4, 5, 8-11], critical thermal loads ΔT_{cr} is reached at first buckling mode $(m,n) = (1,1)$. Because material properties depend on temperature, critical thermal loads and post-buckling curves are traced adopting an iterative algorithm the specific steps of which have been indicated in the preceding studies, for examples [11, 14].

5. Results and discussion

Parametric studies are implemented for FGM plates made of Si_3N_4 and SUS304. The properties of these constituents depend on temperature and are expressed as [42]

$$P = P_0\left(P_{-1}T^{-1} + 1 + P_1T + P_2T^2 + P_3T^3\right) \quad (22)$$

in which $T = T_0 + \Delta T$ with $T_0 = 300K$ and coefficients P_{-1}, P_0, P_1, P_2 and P_3 are given in the Table 1. In numerical examples Poisson's coefficients of the considered materials as well as FGM are hypothesized to be $\nu = 0.29$.

Table 1. Coefficients in Eq. (22) of the properties of constitutive materials [43]

Material	Property	P_0	P_{-1}	P_1	P_2	P_3
Si_3N_4	E_c (Pa)	348.43e+9	0	−3.070e−4	2.160e−7	−8.946e−11
	α_c (1/K)	5.8723e−6	0	9.095e−4	0	0
SUS304	E_m (Pa)	201.04e+9	0	3.079e−4	−6.534e−7	0
	α_m (1/K)	12.330e−6	0	8.086e−4	0	0

5.1. Verification

There are no previous studies on thermally induced instability and post-buckling behavior of FGM plates on elastic foundations with porosity and elastically constrained edges in the literature. Therefore, comparative studies are carried out for special cases of material and structural models. Specifically, buckling behavior of perfect FGM plates ($\xi = 0$) with fully immovable edges and without elastic foundations under uniform temperature rise is considered.

In this comparison, FGM plate is made of aluminum (Al) and alumina (Al_2O_3) with temperature independent properties are $E_m = 70$ GPa, $\alpha_m = 23\times10^{-6}\,(1/°C)$, $\nu_m = 0.3$ for Al and $E_c = 380$ GPa, $\alpha_c = 7.4\times10^{-6}\,(1/°C)$, $\nu_c = 0.3$ for Al_2O_3. Critical buckling temperatures of Al/Al_2O_3

plates with different values of geometry ratios and volume fraction index are sought utilizing explicit-form relation (21) and compared with results obtained by Shariat and Eslami [2] and Lanhe [10] using adjacent equilibrium criterion in the Table 2 and shown along with results of Tran et al. [13] making use of isogeometric approach in Table 3. In these Tables, N^* is volume fraction index in case of FGM plates with metal-rich top plane and ceramic-rich bottom plane, specifically $V_c = (1/2 + z/h)^{N^*}$. It is clear that a very good agreement is obtained in the implemented comparative studies.

In the subsequent subsections, parametric studies on thermal buckling and post-buckling behaviors will be executed. In the presented analyses, degrees of in-plane edge constraints are assessed by dimensionless in-plane stiffness parameters λ_1, λ_2 defined as [14]

$$\lambda_1 = \frac{c_1}{c_1 + E_1^0}, \ \lambda_2 = \frac{c_2}{c_2 + E_1^0} \tag{23}$$

where E_1^0 is value E_1 calculated at room temperature $T_0 = 300\,K$. According to this definition, values of $\lambda_1 = 0$ (i.e. $c_1 = 0$), $\lambda_1 = 1$ (i.e. $c_1 \to \infty$) and $0 < \lambda_1 < 1$ (i.e. $0 < c_1 < \infty$) represent movable, immovable and partially movable cases of edges $x = 0, a$, respectively. Similarly, movable, immovable and partially movable cases of edges $y = 0, b$ are characterized by values of $\lambda_2 = 0$ (i.e. $c_2 = 0$), $\lambda_2 = 1$ (i.e. $c_2 \to \infty$) and $0 < \lambda_2 < 1$ (i.e. $0 < c_2 < \infty$), respectively. In addition, influences of elastic foundations are evaluated by non-dimensional stiffness parameters K_1, K_2 computed in Eq. (A3) in the Appendix section. For the purpose of concise expression, FGM plates are assumed to be square ($a/b = 1$), with perfect geometry ($\mu = 0$), and free from foundation interaction ($K_1 = K_2 = 0$).

5.2. Linear buckling analysis

Parametric studies on linear buckling analysis of perfect FGM plates with pore imperfection are carried out in the present subsection. First of all, the effects of volume percentage ξ of pores, pattern of pore distribution and volume fraction index N on the critical temperatures of FGM plates with immovable condition at boundary edges are shown in Fig. 3. It is noticeable to comment that the critical thermal loadings ΔT_{cr} are enhanced in case the ξ is augmented. In another expression, pores beneficially influence on the buckling withstanding ability of FGM plates under uniform temperature rise. This result can be interpreted that the thermal expansion coefficient of FGM is decreased due to the increase in the ξ. Fig. 3 also indicates that critical thermal loadings are larger when the pores are distributed into the FGM plate according to even type. Discrepancy between critical thermal loadings corresponding to two patterns of porosity distribution is bigger as ξ and/or N become larger.

Table 2. Comparisons of critical thermal loadings ΔT_{cr} ($^\circ C$) of Al/Al_2O_3 rectangular plates with fully immovable boundary edges subjected to uniform temperature rise ($N^* = 1, \xi = 0$).

a / b	Reference, Theory	b / h				
		20	40	60	80	100
0.5	Ref. [10], FSDT	484.51	123.36	55.01	30.98	19.84
	Ref. [2], HSDT	482.18	123.21	54.98	30.97	19.84
	Present, FSDT	482.18	123.21	54.98	30.97	19.84
0.25	Ref. [10], FSDT	1557.1	413.33	185.83	104.95	67.30
	Ref. [2], HSDT	1533.6	411.63	185.48	104.84	67.25
	Present, FSDT	1533.4	411.63	185.48	104.84	67.25

Table 3. Comparisons of critical thermal loadings ΔT_{cr} (°C) of Al/Al_2O_3 square plates with fully immovable edges under uniform temperature rise ($a/b=1$, $\xi=0$).

a / h	Reference	N*					
		0	0.5	1	4	5	10
10	Tran et al. [13]	1618.75	923.20	758.43	670.46	679.34	692.72
	Present	1618.60	922.47	758.37	676.44	686.78	701.08
100	Tran et al. [13]	17.0913	9.6842	7.9409	7.1322	7.2614	7.4641
	Present	17.0895	9.6830	7.9400	7.1322	7.2615	7.4644

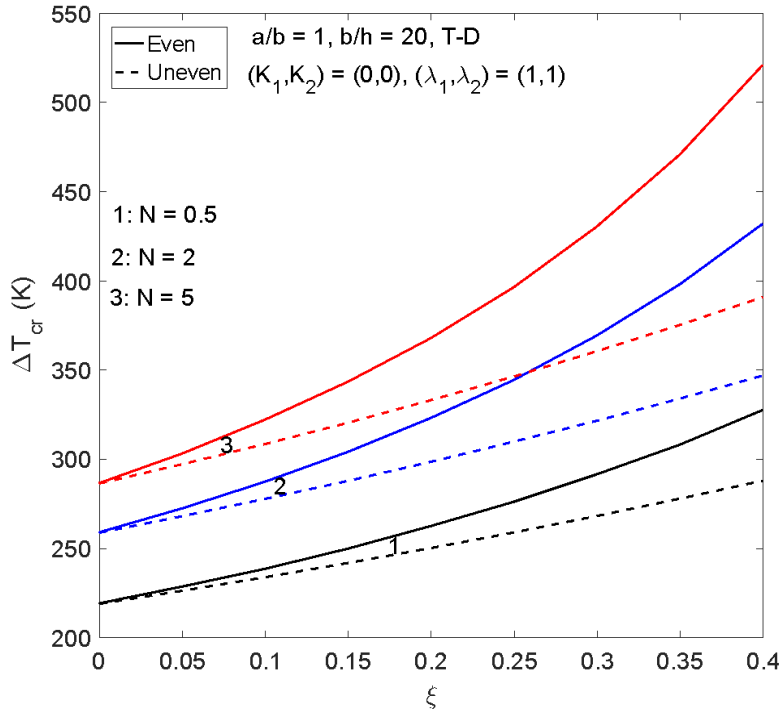

Fig. 3. Effects of N index and porosity volume fraction on critical thermal loads of porous FGM plates with fully immovable condition of edges

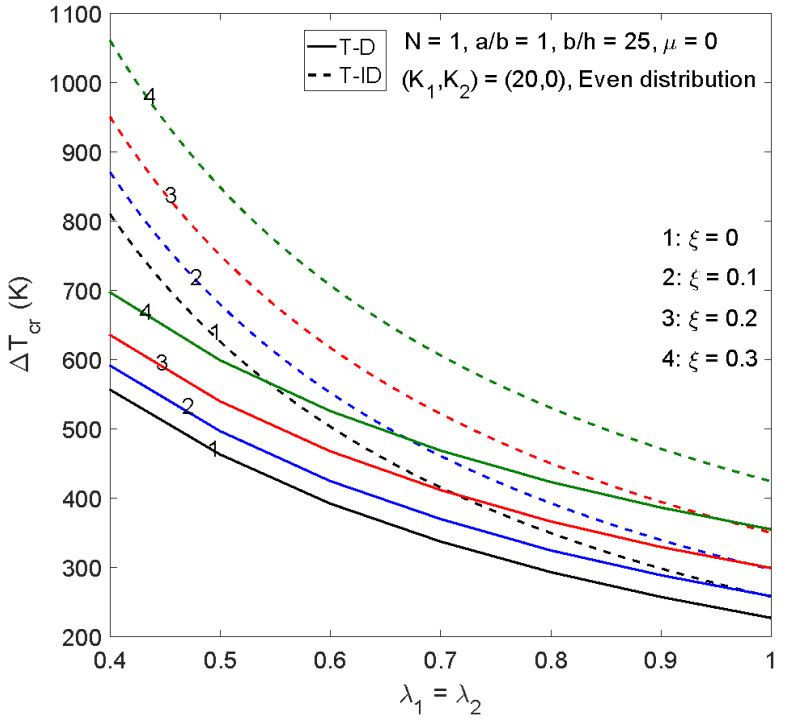

Fig. 4. Effects of tangential edge restraints and porosity percentage on critical thermal loadings of FGM plate with even porosity

Subsequently, the effects of tangential constraints of boundary edges on the critical thermal loads ΔT_{cr} of FGM plates reposing on a Winkler foundation ($K_1 = 20, K_2 = 0$) with evenly distributed pores are considered in Fig. 4 graphed with different values of ξ. As can be seen, the critical thermal loads ΔT_{cr} are substantially reduced when tangential stiffness parameters λ_1, λ_2 are increased. It is shown that temperature–dependent (T-D) properties have evidently harmful effects on the ΔT_{cr}. Discrepancy between values ΔT_{cr} including T-D and temperature–independent (T-ID) properties becomes considerably bigger when parameters λ_1, λ_2 are smaller and/or ξ is larger. Ultimate parametric analysis in this subsection is exhibited in the Table 4 looking at the influences of geometry aspects a/b, b/h and non-dimensional stiffness parameters K_1, K_2 on the critical thermal loadings ΔT_{cr} of FGM plates with immovable boundary edges and evenly distributed pores. As can be observed, ΔT_{cr} is pronouncedly lowered as a/b and/or b/h are larger. In contrast, the elastic foundations obviously improve the thermal buckling resistance capability of porous FGM plates. Additionally, it is realized that difference between results with T-D and T-ID properties is marginal as geometry ratios a/b, b/h are enough large.

5.3. Post-buckling behavior analysis

First example for post-buckling behavior analysis is indicated in Fig. 5 examining the effects of type of pore distribution on thermal post-buckling response of FG rectangular plates with perfect and imperfect geometries along with immovable boundary edges. It is clear that thermal load – transverse displacement equilibrium curve of porous FGM plate ($\xi = 0.2$) is higher than that of perfect FGM plate ($\xi = 0$). Moreover, thermally loaded FGM plate is more stable when porosities are distributed within the FGM plate according to even pattern. Subsequently, the effects of volume percentage ξ of pores on the thermal nonlinear instability response of FGM plates with even pores and immovable edges are depicted in Fig. 6. Generally, porosity beneficially affects the loading withstanding capability of thermally loaded FGM plates and temperature – deflection path is higher when ξ becomes larger. More concretely, post-buckling path is slightly enhanced when ξ is increased from 0 to 0.1 and then significantly higher as ξ varies from 0.1 to 0.3.

Table 4. Effects of geometry ratios and elastic foundations on critical thermal loadings ΔT_{cr} (K) of FGM plates with even pores ($N = 2, \xi = 0.2, \lambda_1 = \lambda_2 = 1$).

a / b	K_1, K_2	b / h			
		20	30	40	50
1	(0,0)	322.75 (395.81)	159.53 (177.21)	93.85 (99.94)	61.50 (64.04)
	(10,0)	400.24 (502.59)	199.14 (224.67)	117.71 (126.63)	77.24 (81.12)
	(5,1)	511.55 (659.98)	255.59 (294.62)	151.91 (165.98)	100.12 (106.31)
1.5	(0,0)	245.02 (286.91)	118.45 (128.20)	69.00 (72.25)	44.89 (46.28)
	(10,0)	357.56 (434.76)	175.03 (193.91)	102.71 (109.21)	67.16 (69.93)
	(5,1)	457.93 (571.62)	225.46 (254.73)	132.96 (143.42)	87.33 (91.83)
2	(0,0)	216.11 (248.61)	103.56 (111.00)	60.02 (62.54)	38.99 (40.06)
	(10,0)	348.46 (419.46)	169.62 (186.94)	99.26 (105.25)	64.82 (67.39)
	(5,1)	441.45 (544.81)	216.11 (242.65)	127.18 (136.59)	83.39 (87.45)

Numbers in brackets indicate results calculated with T-ID properties.

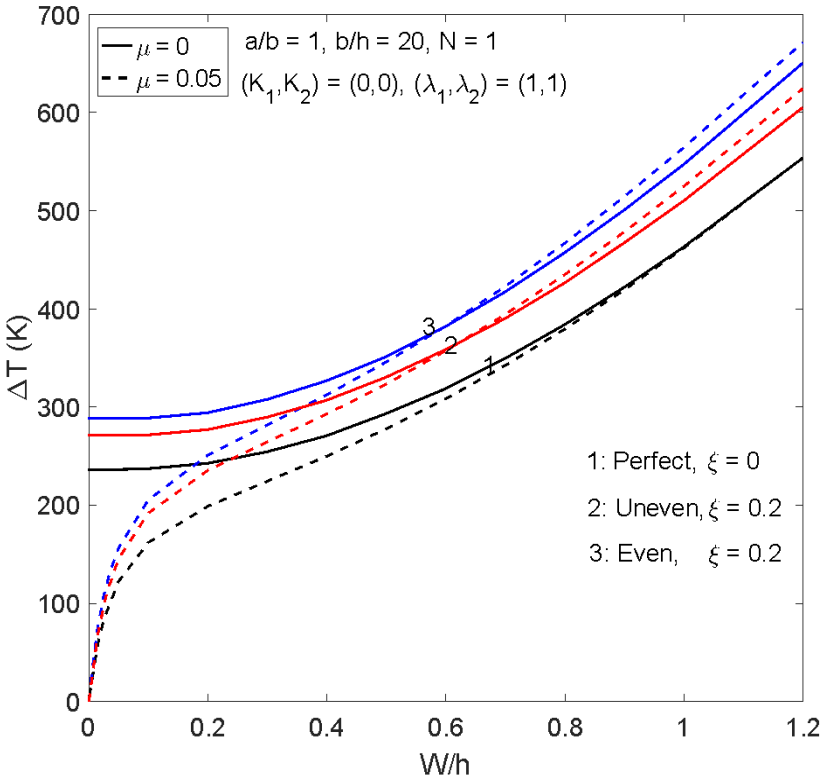

Fig. 5. Effects of porosity distribution pattern on the thermal post-buckling behavior of FGM plates with immovable edges

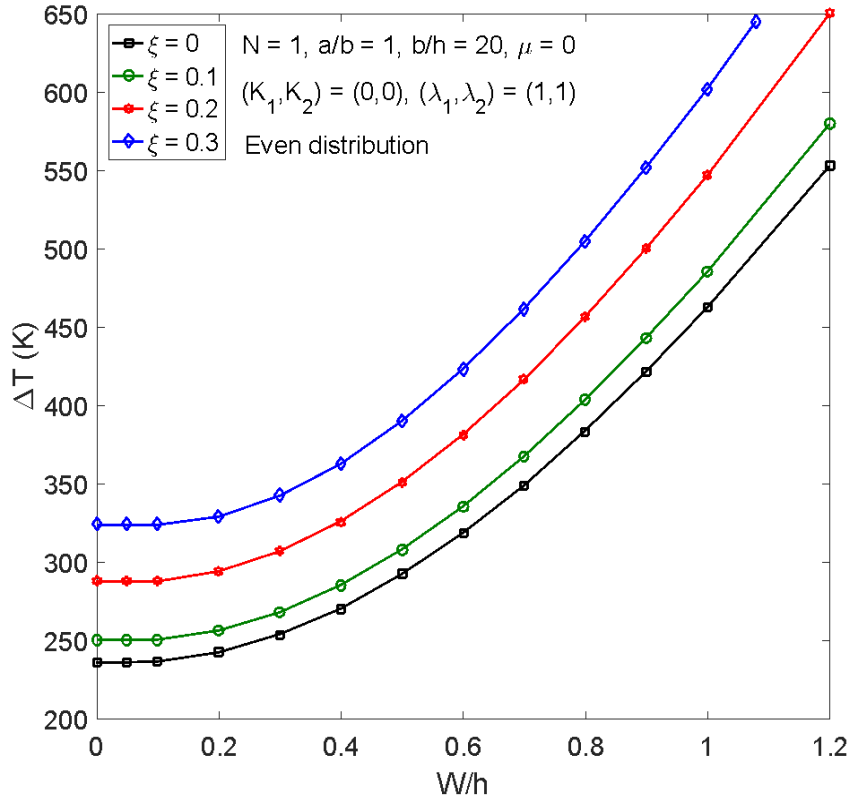

Fig. 6. Effects of porosity volume fraction on the post-buckling curves of FGM plates with immovable edges and even type of pore distribution.

Next numerical example is displayed in Fig. 7 evaluating the influences of volume fraction index N on the nonlinear instability of FGM plates with evenly distributed pores and immovable boundary edges under thermal load. It is evident that the post-buckling load bearing capacity of the plate is higher as N is larger. Additionally, the harmful effect of T-D properties on thermal loading capacity in the post-buckling regions is more pronounced as N is higher (i.e. higher ratio of ceramic).

Subsequently, the influences of tangential restraints of boundary edges on the nonlinear instability behavior of porous FGM plates are exhibited in Fig. 8 plotted with various three couples of parameters λ_1, λ_2. It can be found that, the post-buckling paths are substantially dropped as a result of increase in parameters λ_1, λ_2. It can be interpreted that thermal reactive compressive forces at boundary edges are larger as the boundary edges are more intensely constrained. Furthermore, equilibrium paths accounting for T-D and T-ID properties are closer for larger values of parameters λ_1, λ_2.

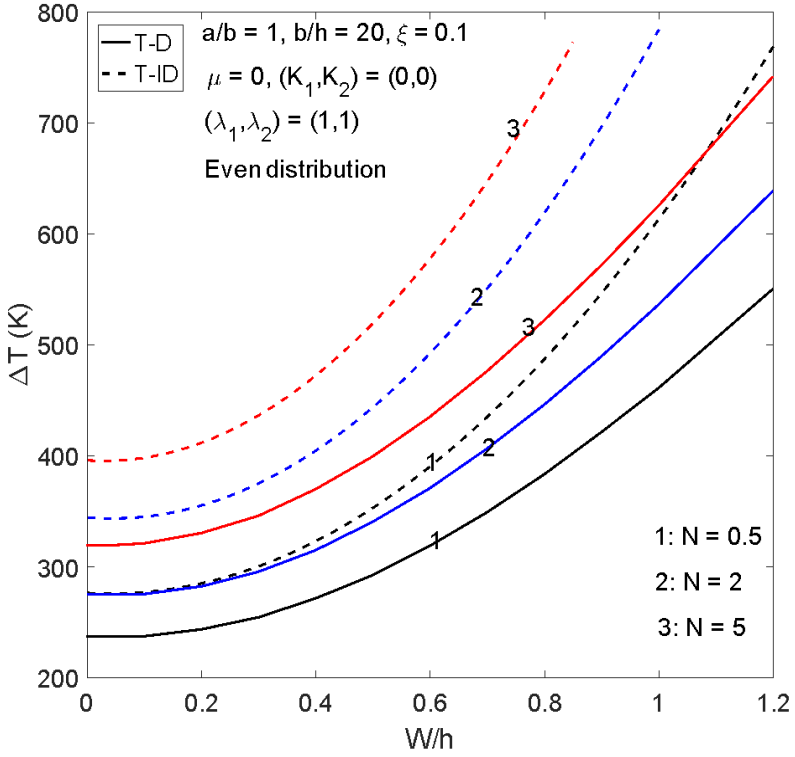

Fig. 7. Effects of volume fraction index on the post-buckling curves of FGM plates with immovable edges and evenly distributed pores

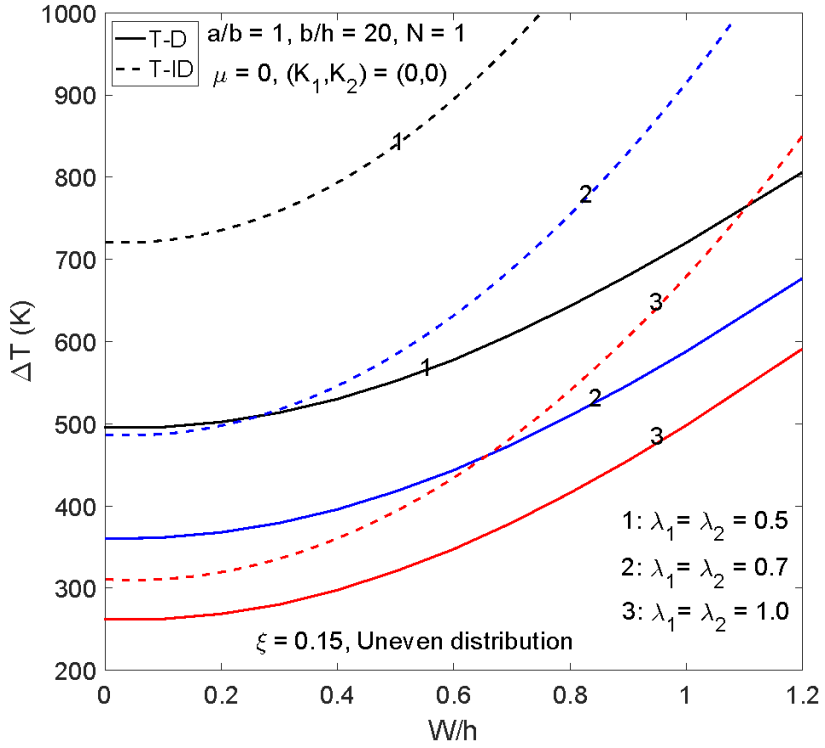

Fig. 8. Effects of tangential edge constraints on the post-buckling curves of FGM plates with unevenly distributed pores

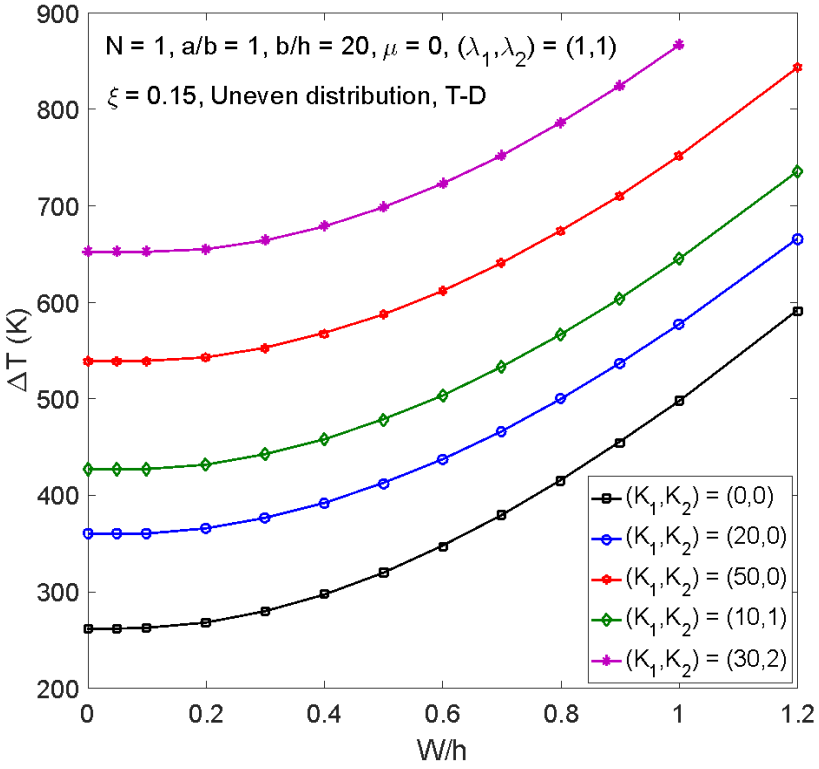

Fig. 9. Effects of foundation interaction on the thermally induced nonlinear instability of FGM plates with unevenly distributed pores

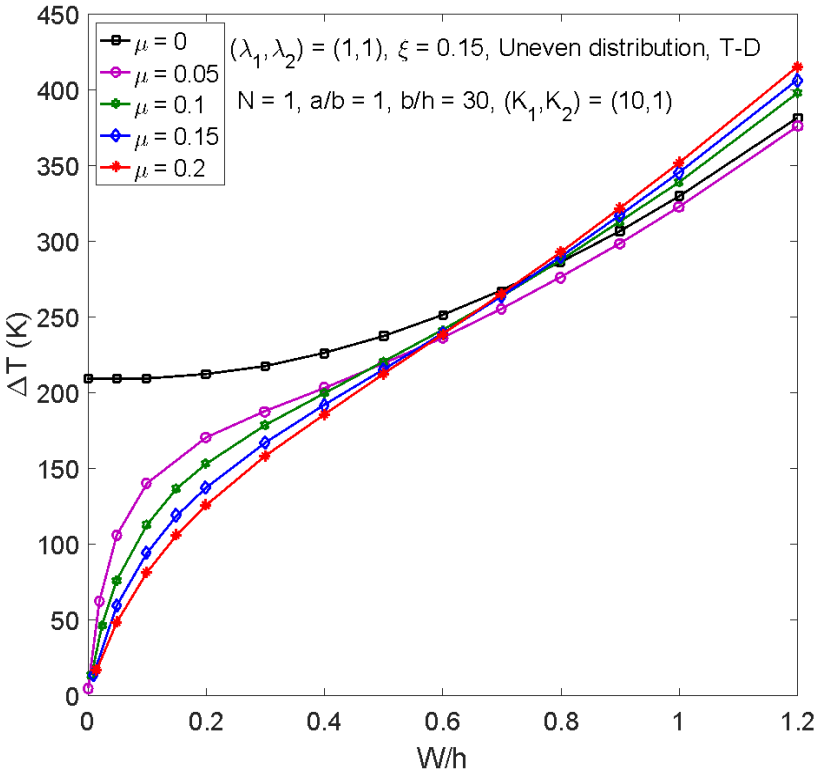

Fig. 10. Effects of initial geometric imperfection on the thermal post-buckling behavior of FGM plates with uneven porosites

Next, the effects of elastic foundations on the thermal post-buckling response of FGM plates with unevenly distributed pores are illustrated in Fig. 9 graphed with different five couples of parameters K_1,K_2. As can be observed, the support of elastic foundations leads to positive efficiency of loading carrying and post-buckling strength is substantially increased as a result of enhancements of parameters K_1,K_2.

Subsequently, Fig. 10 examines the impacts of initial geometric imperfection on the thermally induced nonlinear instability of porous FGM plates resting on a Pasternak-type foundation with immovable condition of all boundary edges. As can

be observed, the presence of geometrical imperfection lowers the loading bearing capacity of the plate when the deflection is small. However, geometrical imperfection positively affects the nonlinear stability of thermally loaded plates as the transverse displacement is sufficiently larger.

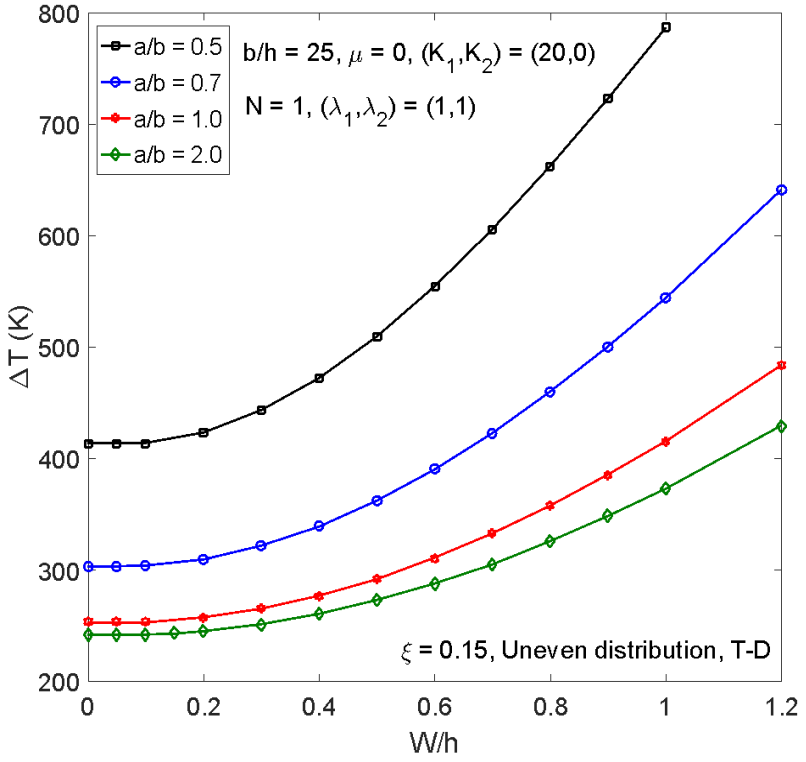

Fig. 11. Effects of aspect ratio on the thermal post-buckling curves of FGM plates with uneven type of porosity distribution

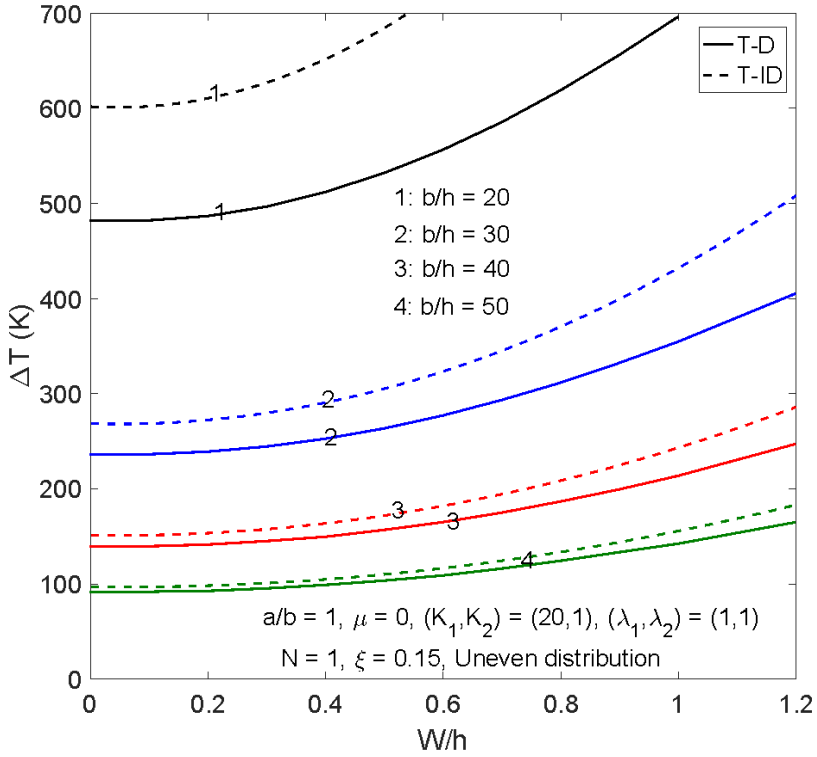

Fig. 12. Effects of width-to-thickness ratio on the thermal post-buckling behavior of FGM plates with uneven pattern of porosity distribution

Subsequent examination is exhibited in Fig. 11 looking at the effects of aspect ratio a/b on the nonlinear instability behavior of porous FGM plates reposing on a Winkler-type foundation subjected to uniform temperature rise. As shown, the post-buckling strength is quickly reduced when a/b is increased from 0.5 to 1 and then slowly lowered as a/b increases from 1 to 2. In addition, the

temperature-deflection equilibrium paths are developed more gradually in case a/b ratio is augmented.

Finally, the influences of b/h ratio of width-to-thickness on the thermal post-buckling response of porous FGM plates resting on a Pasternak-type foundation exposed to uniform temperature rise are evaluated in Fig. 12. It is recognized that post-buckling temperature bearing capability of the plate are significantly weakened when b/h ratio is larger. Furthermore, the effect of T-D properties on predictions of post-buckling response can be marginal when the plate is very thin.

6. Concluding remarks

The numerous effects of porosity, tangential edge restraints and foundation interaction on the buckling and post-buckling behaviors of FGM plates exposed to uniform temperature rise have been examined. The above analyses result in the following conclusions:

Pores have positive effects on the nonlinear stability of FGM rectangular plates subjected to thermal loads. Critical temperatures and post-buckling strength are enhanced due to the existence of porosities.

Thermally loaded FGM plate is more stable as pores are distributed into the FGM plate through even pattern. Positive influence of even distribution pattern is more pronounced as the ceramic percentage is larger.

Tangential restraints of boundary edges have sensitive and remarkable effects on the thermal instability of porous FGM plates. Generally, buckling temperature is lower and post-buckling strength is pronouncedly weaker as the edges are restrained more rigorously.

References

[1] X. Zhao, Y.Y. Lee, K.M. Liew. (2009). Mechanical and thermal buckling analysis of functionally graded plates. *Composite Structures*, 90(2), 161-171. https://doi.org/10.1016/j.compstruct.2009.03.005

[2] B.A. Samsam Shariat, M.R. Eslami. (2007). Buckling of thick functionally graded plates under mechanical and thermal loads. *Composite Structures*, 78(3), 433-439. https://doi.org/10.1016/j.compstruct.2005.11.001

[3] H.-T. Thai, S.-E. Kim. (2013). Closed-form solution for buckling analysis of thick functionally graded plates on elastic foundation. *International Journal of Mechanical Sciences*, 75, 34-44. https://doi.org/10.1016/j.ijmecsci.2013.06.007

[4] H.V. Tung, N.D. Duc. (2010). Nonlinear analysis of stability for functionally graded plates under mechanical and thermal loads. *Composite Structures*, 92(5), 1184-1191. https://doi.org/10.1016/j.compstruct.2009.10.015

[5] N.D. Duc, H.V. Tung. (2011). Mechanical and thermal postbuckling of higher order shear deformable functionally graded plates on elastic foundations. *Composite Structures*, 93(11), 2874-2881. https://doi.org/10.1016/j.compstruct.2011.05.017

[6] R. Kandasamy, R. Dimitri, F. Tornabene. (2016). Numerical study on the free vibration and thermal buckling behavior of moderately thick functionally graded structures in thermal environments. *Composite Structures*, 157, 207-221.

[7] A. Tati. (2021). Finite element analysis of thermal and mechanical buckling behavior of functionally graded plates. *Archive of Applied Mechanics*, 91, 4571-4587. https://doi.org/10.1007/s00419-021-02025-w

[8] R. Javaheri, M.R. Eslami. (2002). Thermal buckling of functionally graded plates. *AIAA Journal*, 40(1), 162-169. https://doi.org/10.2514/2.1626

[9] R. Javaheri, M.R. Eslami. (2002). Thermal buckling of functionally graded plates based on higher order theory. *Journal of Thermal*

Stresses, 25(7), 603-625. https://doi.org/10.1080/01495730290074333

[10] W. Lanhe. (2004). Thermal buckling of a simply supported moderately thick rectangular FGM plate. *Composite Structures*, 64(2), 211-218. https://doi.org/10.1016/j.compstruct.2003.08.004

[11] H.-S. Shen. (2007). Thermal postbuckling behavior of shear deformable FGM plates with temperature-dependent properties. *International Journal of Mechanical Sciences*, 49(4), 466-478. https://doi.org/10.1016/j.ijmecsci.2006.09.011

[12] M. Bodaghi, A.R. Saidi. (2011). Thermoelastic buckling behavior of thick functionally graded rectangular plates. *Archive of Applied Mechanics*, 81, 1555-1572. https://doi.org/10.1007/s00419-010-0501-0

[13] L.V. Tran, C.H. Thai, H.X. Nguyen. (2013). An isogeometric finite element formulation for thermal buckling analysis of functionally graded plates. *Finite Elements in Analysis and Design*, 73, 65-76. https://doi.org/10.1016/j.finel.2013.05.003

[14] H.V. Tung. (2015). Thermal and thermomechanical postbuckling of FGM sandwich plates resting on elastic foundations with tangential edge constraints and temperature dependent properties. *Composite Structures*, 131, 1028-1039. https://doi.org/10.1016/j.compstruct.2015.06.043

[15] S. Trabelsi, A. Frikha, S. Zghal, F. Dammak. (2019). A modified FSDT-based four nodes finite shell element for thermal buckling analysis of functionally graded plates and cylindrical shells. *Engineering Structures*, 178, 444-459. https://doi.org/10.1016/j.engstruct.2018.10.047

[16] S. Trabelsi, A. Frikha, S. Zghal, F. Dammak. (2018). Thermal post-buckling analysis of functionally graded material structures using a modified FSDT. *International Journal of Mechanical Sciences*, 144, 74-89. https://doi.org/10.1016/j.ijmecsci.2018.05.033

[17] A. Hajlaoui, E. Chebbi, F. Dammak. (2021). Three-dimensional thermal buckling analysis of functionally graded material structures using a modified FSDT-based solid-shell element. *International Journal of Pressure Vessels and Piping*, 194, 104547. https://doi.org/10.1016/j.ijpvp.2021.104547

[18] V.N.V. Do, C.-H. Lee. (2018). Quasi-3D higher-order shear deformation theory for thermal buckling analysis of FGM plates based on meshless method. *Aerospace Science and Technology*, 82-83, 450-465. https://doi.org/10.1016/j.ast.2018.09.017

[19] D.T. Dong, V.H. Nam, N.T. Trung, N.T.H. Phuong, V.T. Hung. (2020). Nonlinear thermomechanical buckling of sandwich FGM oblique stiffened plates with nonlinear effect of elastic foundation. *Journal of Thermoplastic Composite Materials*, 35, 1441-1467. DOI:10.1177/0892705720935957

[20] H.S. Shen, C.L. Zhang. (2010). Thermal buckling and postbuckling behavior of functionally graded carbon nanotube-reinforced composite plates. *Materials & Design*, 31(7), 3403-3411. https://doi.org/10.1016/j.matdes.2010.01.048

[21] M. Mirzaei, Y. Kiani. (2016). Thermal buckling of temperature dependent FG-CNT reinforced composite plates. *Meccanica*, 51(9), 2185-2201. https://doi.org/10.1007/s11012-015-0348-0

[22] Y. Kiani. (2017). Thermal post-buckling of FG-CNT reinforced composite plates. *Composite Structures*, 159, 299-306. https://doi.org/10.1016/j.compstruct.2016.09.084

[23] H.V. Tung. (2017). Thermal buckling and postbuckling behavior of functionally graded carbon nanotube-reinforced composite plates resting on elastic foundations with tangential edge restraints. *Journal of Thermal Stresses*, 40(5), 641-663. https://doi.org/10.1080/01495739.2016.12545

77

[24] H.V. Tung, L.T.N. Trang. (2020). Thermal postbuckling of shear deformable CNT-reinforced composite plates with tangentially restrained edges and temperature dependent properties. *Journal of Thermoplastic Composite Materials*, 33(1), 97-124.

[25] L.T.N. Trang, H.V. Tung. (2022). Thermally induced postbuckling of thin CNT-reinforced composite plates under nonuniform in-plane temperature distributions. *Journal of Thermoplastic Composite Materials*, 35(12), 2331-2353.

[26] N. Wattanasakulpong, V. Ungbhakorn. (2014). Linear and nonlinear vibration analysis of elastically restrained ends FGM beams with porosities. *Aerospace Science and Technology*, 32(1), 111-120. https://doi.org/10.1016/j.ast.2013.12.002

[27] N.D. Anh, N.V. Thinh, H.V. Tung. (2024). Nonlinear vibration analysis of geometrically imperfect FGM Timoshenko beams with porosity and elastically restrained ends in thermal environments. *Mechanics Based Design of Structures and Machines*, 52(12), 10148-10169. https://doi.org/10.1080/15397734.2024.2353876

[28] A. Gupta, M. Talha. (2018). Influence of initial geometric imperfections and porosity on the stability of functionally graded material plates. *Mechanics Based Design of Structures and Machines*, 46(6), 693-711. https://doi.org/10.1080/15397734.2018.1449656

[29] P.H. Cong, T.M. Chien, N.D. Khoa, N.D. Duc. (2018). Nonlinear thermomechanical buckling and post-buckling response of porous FGM plates using Reddy's HSDT. *Aerospace Science and Technology*, 77, 419-428. https://doi.org/10.1016/j.ast.2018.03.020

[30] M.-C. Trinh, T. Mukhopadhyay, S.-E. Kim. (2020). A semi-analytical stochastic buckling quantification of porous functionally graded plates. *Aerospace Science and Technology*, 105, 105928. https://doi.org/10.1016/j.ast.2020.105928

[31] L.T. Cuong, T.V. Loc, B.Q. Tinh, N.X. Hoang, M.A. Wahab. (2019). Isogeometric analysis for size-dependent nonlinear thermal stability of porous FG microplates. *Composite Structures*, 221, 110838. https://doi.org/10.1016/j.compstruct.2019.04.010

[32] E. Salari, S.A. Sadough Vanini, A.R. Ashoori, A.H. Akbarzadeh. (2020). Nonlinear thermal behavior of shear deformable FG porous nanobeams with geometrical imperfection: Snap-through and postbuckling analysis. *International Journal of Mechanical Sciences*, 178, 105615. https://doi.org/10.1016/j.ijmecsci.2020.105615

[33] M. Dhuria, N. Grover, K. Goyal. (2021). Influence of porosity distribution on static and buckling responses of porous functionally graded plates. *Structures*, 34, 1458-1474. https://doi.org/10.1016/j.istruc.2021.08.050

[34] N.T. Phuong, V.H. Nam, B.T. Tu. (2025). An analytical approach for nonlinear thermo-mechanical buckling behavior of porous FG-GPLRC circular plates and spherical caps. *Journal of Science and Transport Technology*, 5(1), 40-60. https://doi.org/10.58845/jstt.utt.2025.en.5.1.40-60

[35] N.H. Quan, V.M. Duc, N.T. Phuong, L.N. Ly, N.T.M. Trang. (2022). Buckling behavior of spiral stiffened sandwich FGM cylindrical shells with porous core under axial compression using the FSDT. *Journal of Science and Transport Technology*, 2(3), 1-9. https://doi.org/10.58845/jstt.utt.2022.en.2.3.1-9

[36] V.T. Long, H.V Tung. (2021). Thermal nonlinear buckling of shear deformable functionally graded cylindrical shells with porosities. *AIAA Journal*, 59(6), 2233-2241. https://doi.org/10.2514/1.J060026

[37] V.T. Long, H.V. Tung. (2021).

Thermomechanical nonlinear buckling of pressurized shear deformable FGM cylindrical shells including porosities and elastically restrained edges. *Journal of Aerospace Engineering*, 34(3), 04021011. https://doi.org/10.1061/(ASCE)AS.1943-5525.0001252

[38] V.T. Long, H.V. Tung. (2022). Buckling behavior of thick porous functionally graded material toroidal shell segments under external pressure and elevated temperature including tangential edge restraint. *Journal of Pressure Vessel Technology*, 144(5), 051310. https://doi.org/10.1115/1.4053485

[39] V.T. Long, H.V. Tung. (2023). Postbuckling responses of porous FGM spherical caps and circular plates including edge constraints and nonlinear three-parameter elastic foundations. *Mechanics Based Design of Structures and Machines*, 51(8), 4214-4236. https://doi.org/10.1080/15397734.2021.1956327

[40] N.V. Thinh, H.V. Tung. (2025). Nonlinear thermal vibration and postbuckling of shear deformable porous FGM circular plates with geometric imperfection and elastic edge restraint. *Mechanics Based Design of Structures and Machines*, 53(10), 6765-6788. https://doi.org/10.1080/15397734.2025.2489068

[41] H.V. Tung, L.T.N. Trang. (2021). Nonlinear stability of advanced sandwich cylindrical shells comprising porous functionally graded material and carbon nanotube reinforced composite layers under elevated temperature. *Applied Mathematics and Mechanics (English Edition)*, 42, 1327-1348. https://doi.org/10.1007/s10483-021-2771-6

[42] Y.S. Touloukian. (1967). Thermophysical properties of high temperature solid materials. *New York: MacMillan.*

[43] J.N. Reddy, C.D. Chin. (1998). Thermomechanical analysis of functionally graded cylinders and plates. *Journal of Thermal Stresses*, 21(6), 593-626.https://doi.org/10.1080/01495739808956165

Appendix

+ The specific formulae of coefficients d_{ij} $(i=1\div 2, j=1\div 3)$ in the Eq. (16) are given as the below

$$d_{11}=D\beta_m^2+\frac{1}{2}D(1-\nu)\delta_n^2+\frac{E_1K_S}{2(1+\nu)};\ d_{12}=d_{21}=\frac{1}{2}D(1+\nu)\beta_m\delta_n;\ d_{13}=-\frac{E_1K_S\beta_m}{2(1+\nu)}$$

$$d_{22}=D\delta_n^2+\frac{1}{2}D(1-\nu)\beta_m^2+\frac{E_1K_S}{2(1+\nu)};\ d_{23}=-\frac{E_1K_S\delta_n}{2(1+\nu)} \quad (A1)$$

+ The detailed expressions of coefficients a_{k1} $(k=1\div 3)$ in the Eq. (17) are given as

$$a_{11}=\frac{mn\pi^6}{16B_h^4}\bar{D}\left(m^2B_a^2+n^2\right)^2+\frac{a_{21}E_m^0}{\pi^2B_h^2}\left[K_1+K_2\pi^2\left(m^2B_a^2+n^2\right)\right]$$

$$a_{21}=\frac{mn\pi^4}{16B_h^2}\left[\frac{2\pi^2\bar{D}}{\bar{E}_1K_SB_h^2}(1+\nu)\left(m^2B_a^2+n^2\right)+1\right]$$

$$a_{31}=\left(m^4B_a^4+n^4\right)\left[\frac{mn\bar{D}\pi^8}{128K_SB_h^6}(1+\nu)\left(m^2B_a^2+n^2\right)+\frac{mn\bar{E}_1\pi^6}{256B_h^4}\right] \quad (A2)$$

where

$$\bar{E}_1=\frac{E_1}{h};\ B_h=\frac{b}{h};\ \bar{D}=\frac{D}{h^3};\ (K_1,K_2)=\frac{b^2}{E_m^0h^3}\left(k_1b^2,k_2\right) \quad (A3)$$

with E_m^0 is value of E_m corresponding to $T=300\,K$.

+ The specifics of s_{ij} $(i=1\div 2, j=1\div 3)$ in the Eqs. (19) are displayed as the below

$$s_{11}=-\frac{4\bar{c}_1\bar{E}_2\left[\left(\bar{E}_1+\bar{c}_2\right)mB_a\bar{B}_1+\nu n\bar{c}_2\bar{B}_2\right]}{mn\pi B_h\left[\left(\bar{E}_1+\bar{c}_1\right)\left(\bar{E}_1+\bar{c}_2\right)-\nu^2\bar{c}_1\bar{c}_2\right]};\ s_{12}=\frac{\bar{c}_1\bar{E}_1\pi^2\left[\left(\bar{E}_1+\bar{c}_2\right)m^2B_a^2+\nu n^2\bar{c}_2\right]}{8B_h^2\left[\left(\bar{E}_1+\bar{c}_1\right)\left(\bar{E}_1+\bar{c}_2\right)-\nu^2\bar{c}_1\bar{c}_2\right]}$$

$$s_{13}=\frac{\bar{c}_1\left(\bar{E}_1+\bar{c}_2\right)+\nu\bar{c}_1\bar{c}_2}{\left(\bar{E}_1+\bar{c}_1\right)\left(\bar{E}_1+\bar{c}_2\right)-\nu^2\bar{c}_1\bar{c}_2};\ s_{21}=-\frac{4\bar{c}_2\bar{E}_2\left[\left(\bar{E}_1+\bar{c}_1\right)n\bar{B}_2+\nu\bar{c}_1mB_a\bar{B}_1\right]}{mn\pi B_h\left[\left(\bar{E}_1+\bar{c}_1\right)\left(\bar{E}_1+\bar{c}_2\right)-\nu^2\bar{c}_1\bar{c}_2\right]}$$

$$s_{22}=\frac{\bar{c}_2\bar{E}_1\pi^2\left[\left(\bar{E}_1+\bar{c}_1\right)n^2+\nu m^2\bar{c}_1B_a^2\right]}{8B_h^2\left[\left(\bar{E}_1+\bar{c}_1\right)\left(\bar{E}_1+\bar{c}_2\right)-\nu^2\bar{c}_1\bar{c}_2\right]};\ s_{23}=\frac{\bar{c}_2\left(\bar{E}_1+\bar{c}_1\right)+\nu\bar{c}_1\bar{c}_2}{\left(\bar{E}_1+\bar{c}_1\right)\left(\bar{E}_1+\bar{c}_2\right)-\nu^2\bar{c}_1\bar{c}_2} \quad (A4)$$

where

$$\bar{E}_2=\frac{E_2}{h^2};\ (\bar{c}_1,\bar{c}_2)=\frac{1}{h}(c_1,c_2);\ \bar{B}_1=\frac{d_{13}\bar{d}_{22}-\bar{d}_{12}d_{23}}{\bar{d}_{11}\bar{d}_{22}-\bar{d}_{12}^2};\ \bar{B}_2=\frac{d_{23}\bar{d}_{11}-\bar{d}_{21}d_{13}}{\bar{d}_{11}\bar{d}_{22}-\bar{d}_{12}^2} \quad (A5)$$

in which

$$\left(\bar{d}_{11},\bar{d}_{12},\bar{d}_{21},\bar{d}_{22}\right)=\frac{1}{h}\left(d_{11},d_{12},d_{21},d_{22}\right) \quad (A6)$$